



HAL
open science

First-principles electronic structure calculations for the whole spinel oxide solid solution range $\text{Mn}_x\text{Co}_{3-x}\text{O}_4$ ($0 \leq x \leq 3$) and their comparison with experimental data

Rémi Arras, Thi Ly Le, Sophie Guillemet-Fritsch, Pascal Dufour, Christophe Tenailleau

► To cite this version:

Rémi Arras, Thi Ly Le, Sophie Guillemet-Fritsch, Pascal Dufour, Christophe Tenailleau. First-principles electronic structure calculations for the whole spinel oxide solid solution range $\text{Mn}_x\text{Co}_{3-x}\text{O}_4$ ($0 \leq x \leq 3$) and their comparison with experimental data. *Physical Chemistry Chemical Physics*, 2016, 18 (37), pp.26166-26176. 10.1039/c6cp05554k . hal-01718308

HAL Id: hal-01718308

<https://hal.science/hal-01718308v1>

Submitted on 1 Feb 2019

HAL is a multi-disciplinary open access archive for the deposit and dissemination of scientific research documents, whether they are published or not. The documents may come from teaching and research institutions in France or abroad, or from public or private research centers.

L'archive ouverte pluridisciplinaire **HAL**, est destinée au dépôt et à la diffusion de documents scientifiques de niveau recherche, publiés ou non, émanant des établissements d'enseignement et de recherche français ou étrangers, des laboratoires publics ou privés.







Open Archive Toulouse Archive Ouverte (OATAO)

OATAO is an open access repository that collects the work of Toulouse researchers and makes it freely available over the web where possible

This is an author's version published in: <http://oatao.univ-toulouse.fr/16785>

Official URL: <https://doi.org/10.1039/c6cp05554k>

To cite this version:

Arras, Rémi and Le, Thi Ly  and Guillemet, Sophie  and Dufour, Pascal 
and Tenailleau, Christophe  *First-principles electronic structure calculations for the whole spinel oxide solid solution range $Mn_xCo_{3-x}O_4$ ($0 \leq x \leq 3$) and their comparison with experimental data.* (2016) *Physical Chemistry Chemical Physics*, 18 (37). 26166-26176. ISSN 1463-9076

Any correspondence concerning this service should be sent to the repository administrator: tech-oatao@listes-diff.inp-toulouse.fr

First-principles electronic structure calculations for the whole spinel oxide solid solution range $\text{Mn}_x\text{Co}_{3-x}\text{O}_4$ ($0 \leq x \leq 3$) and their comparison with experimental data†

Rémi Arras,^{*a} Thi Ly Le,^b Sophie Guillemet-Fritsch,^b Pascal Dufour^b and Christophe Tenailleau^b

Transition metal spinel oxides have recently been suggested for the creation of efficient photovoltaic cells or photocatalysts. These compounds can be easily tuned by doping to adapt their electronic or magnetic properties. However, their cation distribution is very complex and band structures are still a subject of controversy. We propose a complete density functional theory investigation of $\text{Mn}_x\text{Co}_{3-x}\text{O}_4$ compounds, using different approximations in order to explain the variation of these properties as a function of composition (for $0 \leq x \leq 3$) and determine the electronic structure over the whole solid solution range. A detailed study of their atomic structure, magnetic properties and electronic structure is given and compared with experimental data. The unit cell volume calculated for each composition is in agreement with the volume obtained experimentally in ceramics, while a cubic-to-tetragonal structural transition is predicted at $x = 2.0$. An antiferromagnetic to ferrimagnetic behavior is observed at the lowest ordering temperature depending on the composition. The band gap, deduced from our band structure calculations, strongly decreases upon doping of the end members Co_3O_4 and Mn_3O_4 , but is partly restored by the tetragonal distortion. A direct band gap, close to 0.5–0.8 eV, is calculated for $0.25 \leq x \leq 2.25$, justified by inter-metal transitions from Mn ions on octahedral sites.

DOI: 10.1039/c6cp05554k

1 Introduction

Complex transition metal oxides possess a wide range of electronic and magnetic properties which are highly tunable, depending on the considered cationic chemical species, the overall atomic structure and the experimental growth conditions. This makes such materials very interesting for several industrial applications in electronics, sensors and energy converters, also taking into account their advantages in terms of element abundance, low cost and negligible toxicity.

Spinel cobaltites and manganites are interesting photoelectric materials that have already been proposed as promising candidates for the creation of efficient photovoltaic cells¹ or photocatalysts.^{2,3}

Different experimental studies have already shown that such oxides can be prepared as thin films by physical or chemical vapor deposition,⁴ epitaxial growth,^{5–8} electrodeposition,⁹ sol-gel,¹⁰ and spin or dip-coating techniques.¹¹ While the former two allow the formation of very thin (a few nanometers) compact layers, these techniques are usually expensive. The latter three techniques are more appropriate for the formation of homogeneous layers of a few hundreds of nanometers at a very low cost.

Intermediate oxides, with chemical formula $\text{Mn}_x\text{Co}_{3-x}\text{O}_4$ ($0 \leq x \leq 3$), provide a larger number of cations that will directly influence their material properties. Some of the authors of the current paper previously studied the whole solid solution range experimentally, confirming the interest of such materials for various applications in electronics and optical devices, like for example, thermistors and light absorber materials, and highlighting the variations of the crystal structure and conductivity as a function of the chemical composition.^{12,13} The magnetic properties of dense and single phase $\text{Mn}_x\text{Co}_{3-x}\text{O}_4$ ($0 \leq x \leq 3$) ceramics have also been recently experimentally investigated by the same research group.¹⁴ $\text{Mn}_x\text{Co}_{3-x}\text{O}_4$ possesses a net magnetization at low temperatures and the molar Curie constants C_m , deduced from the experimental measurements for ceramics with $0 \leq x \leq 2$, were explained by the presence of two

^a CEMES, Université de Toulouse, CNRS, UPS, 29, rue Jeanne-Marvig, F-31055 Toulouse, France. E-mail: remi.arras@cemes.fr; Tel: +33 562257856

^b CIRIMAT, Université de Toulouse, CNRS, INPT, UPS, 118 Route de Narbonne, 31062 Toulouse Cedex 9, France

† Electronic supplementary information (ESI) available: Detailed DOS of Co_3O_4 (Fig. 1S) and Mn_3O_4 (Fig. 2S and 3S). Volume and lattice parameters of $\text{Mn}_x\text{Co}_{3-x}\text{O}_4$ calculated with the GGA+U approximation (Fig. 4S). Complete sets of DOS of $\text{Mn}_x\text{Co}_{3-x}\text{O}_4$ for the GGA (Fig. 5S), GGA+U (Fig. 6S) and mBJ (Fig. 7S) calculations. DOS calculated using the experimental lattice parameters (Fig. 8S). Variation of the band gaps (Fig. 9S). See DOI: 10.1039/c6cp05554k

oxidation states per element ($\text{Co}^{2+}/\text{Co}^{3+}$ and $\text{Mn}^{3+}/\text{Mn}^{4+}$), which also justifies the conductivity variation.¹²

Few first-principles studies have already been reported for the pure bulk end member compounds Mn_3O_4 ^{15–18} and Co_3O_4 .^{5,6,19–23} In these works, the authors aimed at describing accurately the electronic structures using different approximations for the exchange–correlation potential. Other recent first-principles studies showed the correlation between the spinel oxide electronic structure and the surface and catalytic properties of Co_3O_4 ^{24–27} as well as MnCo_2O_4 .^{28–30}

But, further theoretical and experimental works need to be done in order to obtain a better understanding of the structural, electronic and magnetic properties of such complex oxide materials.

In this paper, after describing the pure end member compounds Co_3O_4 (Section 3.1) and Mn_3O_4 (Section 3.2), we propose a fundamental and complete study of the structural, magnetic and electronic properties of $\text{Mn}_x\text{Co}_{3-x}\text{O}_4$, based on first-principles calculations and in comparison with our previous experimental results (Section 3.3).

2 Calculation details

Our calculations were performed using the density functional theory (DFT) and the projector augmented-wave (PAW) method³¹ with a cut-off energy of 650 eV, as implemented in the Vienna *Ab initio* Simulation Package (VASP).^{32,33} The first Brillouin zone was sampled by a $10 \times 10 \times 10$ Monkhorst–Pack grid.³⁴ A full optimization of the atomic structure (atomic coordinates and volume) was performed for each case using the conjugate-gradient algorithm method and calculating the stress tensor. This step was only done using the exchange–correlation energy approximated by the generalized-gradient approximation (GGA-PBE).³⁵ The electronic structure was then calculated according to the Tran–Blaha modified Becke–Johnson local spin density approximation (mBJ),^{36,37} or by adding the so-called “+ U ” correction,³⁸ applied to the d-electrons of the Mn and Co atoms. We used the rotationally invariant version of this method, as introduced by Dudarev *et al.*³⁹ and the $U_{\text{eff}}(=U - J)$ parameter was chosen to be 5.0 eV and 3.8 eV, for the Co and Mn atoms, respectively. Since the mBJ potential is not obtained as a derivative of the exchange functional, it is advised not to use it for energy comparison (structural optimization or stability of magnetic states), but only for electronic structure calculations, where this method has been found to improve the description (with a relatively low computational cost) and, in particular, the band gap values for a large range of materials, including transition metal oxides.^{37,40}

3 Results

3.1 Co_3O_4

Co_3O_4 displays a spinel structure, which corresponds to a distorted face-centred cubic lattice of oxygen atoms in which Co atoms occupy 1/8 of the tetrahedral (A) and 1/2 of the octahedral (B) atomic sites. Co_A , Co_B and O atoms occupy,

respectively, the atomic sites 8a, 16d and 32e in the Wyckoff notation. Our calculated value of 8.087 Å is in agreement with the experimental lattice parameter ($a = 8.081$ Å) previously obtained for Co_3O_4 dense ceramics after spark plasma sintering (SPS).¹²

Co_3O_4 is a mixed valence oxide with two oxidation states that provides interesting electronic and magnetic properties. The electronic charge distribution in this material corresponds to the so-called normal spinel structure, which can be described according to the formula $[\text{Co}^{2+}]_A[\text{Co}^{\text{III}}]_B(\text{O}^{2-})_4$. We use the Co_B^{III} notation because cobalt in octahedral sites adopts a low spin state with a nil spin magnetic moment. Co_A^{2+} ions are in a high spin state (with a theoretical spin magnetic moment of $M_S = \pm 3 \mu_B$) and are antiferromagnetically coupled together, with a low Néel temperature of 40 K. In his experimental study, Roth highlighted the strength of the A–A antiferromagnetic indirect coupling that is for example higher than in aluminate spinel compounds.⁴¹ The total spin magnetic moment for Co_3O_4 is of 0 μ_B per formula unit (f.u.), which is correctly described as being the fundamental magnetic state by our calculations, with a total energy of 27 meV per f.u. lower than that calculated for a ferromagnetic ordering, according to the GGA calculations. A spin magnetic moment of 3.26 μ_B was measured by Roth.⁴² This value is higher than the theoretical value of 3 μ_B given before, considering a purely ionic character of the Co^{2+} and the spin only contribution. It is also higher than our calculated value, which is at the most 2.77 μ_B using the mBJ calculations. Roth explained that this high measured value was due to a small contribution from the spin–orbit coupling.⁴²

Regarding the band structure, a debate is still opened with the band gap width of Co_3O_4 at the Fermi level. Most of the results reported in the literature, based on optical measurements mainly, usually describe two band gaps of $\simeq 1.6$ eV and $\simeq 2$ –2.5 eV,^{43–46} while some references also reported a band gap with a lower value of $\simeq 0.8$ eV,^{5,6,19} and thus claim that Co_3O_4 would not be a highly correlated electron material in contrast to the Mott insulator CoO. The last hypothesis would be described within the GGA+ U formalism by using a lower value of U_{eff} for the d electrons, especially for the Co_B^{III} ions. The electronic structure variation for Co_3O_4 as a function of U_{eff} has been described by Qiao *et al.*,⁵ showing that the spinel cobalt oxide electronic structure was better investigated by standard DFT calculations than by using DFT+ U , when compared to X-ray photoelectron spectroscopy (XPS) data. Kormondy *et al.* also mapped several combinations of [$U_{\text{eff}}(\text{Co}_A^{2+})$, $U_{\text{eff}}(\text{Co}_B^{3+})$] and finally chose the set of value of [4.0, 0.0] eV after a comparison of their calculating results with magnetization measurements and XPS spectra. These values are much lower than [4.4, 6.7] eV calculated by Chen *et al.*²⁰ from first-principles, by using a linear response method. As discussed there, the set of parameters still gives a band gap lower by a factor 1.75 than for PBE0 hybrid functional calculations. For comparison, calculated U_{eff} values for CoO are of the order of 5 eV.⁴⁷ Finally, a study performed by Singh *et al.*²² aims at comparing different approximations (GGA-PBE, GGA+ U , and HSE06 as well as many-body Green function GW approximations) to calculate the electronic,

magnetic and optical properties of Co_3O_4 . They highlighted that the results obtained using the GGA+ U and HSE06 hybrid functional are very sensitive to the chosen value of U_{eff} or to the percentage of exact exchange introduced in the exchange–correlation DFT functional. After comparison with photoemission spectroscopy (PES) and ultraviolet photoelectron spectroscopy (UPS), they concluded that the pure GGA functional, the hybrid HSE06 (with a percentage of exact exchange $\alpha = 5\%$) functional, and the Sc-GW0 method (GW with only full self-consistency over G) are the most reliable methods to investigate the electronic and optical properties of Co_3O_4 .

The reason for the low measured band gap is uncertain and was not always discussed. We preferred to keep a high constant value of U_{eff} for every Co atom, in order to be consistent with the mBJ calculations. GGA results will still be given for each system for comparison.

Our band gap widths are then 0.27 eV, 2.33 eV, and 2.91 eV calculated using the GGA, GGA+ U ($U_{\text{eff}} = 5$ eV), and mBJ methods, respectively. These values are in agreement with the theoretical results reported in ref. 21. Densities of states (DOS) are plotted in Fig. 1. The DOS calculated using the GGA+ U method displays a strong hybridization between the d orbitals of Co atoms in A and B sites and the p orbitals of oxygen atoms over the whole range of occupied valence bands, *i.e.* from -7.25 eV to E_F . This mainly results from the energy shift of the d bands toward lower energies, due to the application of the U_{eff} -dependent correction. In contrast, GGA and mBJ calculations show a large separation between bands with a strong d-orbital contribution (respectively from -2.38 eV or -2.12 eV to E_F) and p bands of the O^{2-} anions. This is characteristic of low hybridization and clearly delimitates the respective localization of the electrons near the cations or the oxygen atoms. According to the mBJ calculations, the band gap observed in Co_3O_4 corresponds to the difference in energy between occupied e bands of Co_A and e_g unoccupied bands of Co_B . The difference in energy between the occupied e and unoccupied t_2 bands of Co_A ($\Delta E^A(e \rightarrow t_2)$), and the occupied t_{2g} and unoccupied e_g bands of Co_B ($\Delta E^B(t_{2g} \rightarrow e_g)$) is 5.45 eV and 3.88 eV, respectively, (see Fig. 1S of the ESI[†]).

3.2 Mn_3O_4

Hausmannite Mn_3O_4 crystallizes also with the spinel structural type,⁴⁸ but exhibits a tetragonal distortion with our experimental lattice parameters $a = 8.149$ Å and $c = 9.465$ Å (*i.e.* a c/a ratio equal to 1.162) as previously described for a single phase and dense ceramic.¹² Our calculations here give cell parameter values of $a = 8.132$ Å and $c = 9.493$ Å ($c/a = 1.167$) considering antiferromagnetic ordering, which are again in agreement with the experimental data.

The charge distribution in Mn_3O_4 also corresponds to the normal spinel structure formula $[\text{Mn}^{2+}]_A([\text{Mn}^{3+}]_B(\text{O}^{2-})_4)$ but in this case, with both Mn_A^{2+} ($M_S = 5 \mu_B$) and Mn_B^{3+} ($M_S = 4 \mu_B$) cations in the high-spin state.

Mn_3O_4 exhibits a complex ferrimagnetic ordering below the Curie temperature T_C of approximately 42 K,⁴⁹ below which it undergoes three magnetic phases.^{50–56} Between 39 K and T_C , Mn_3O_4 is reported to be commensurate and collinear,

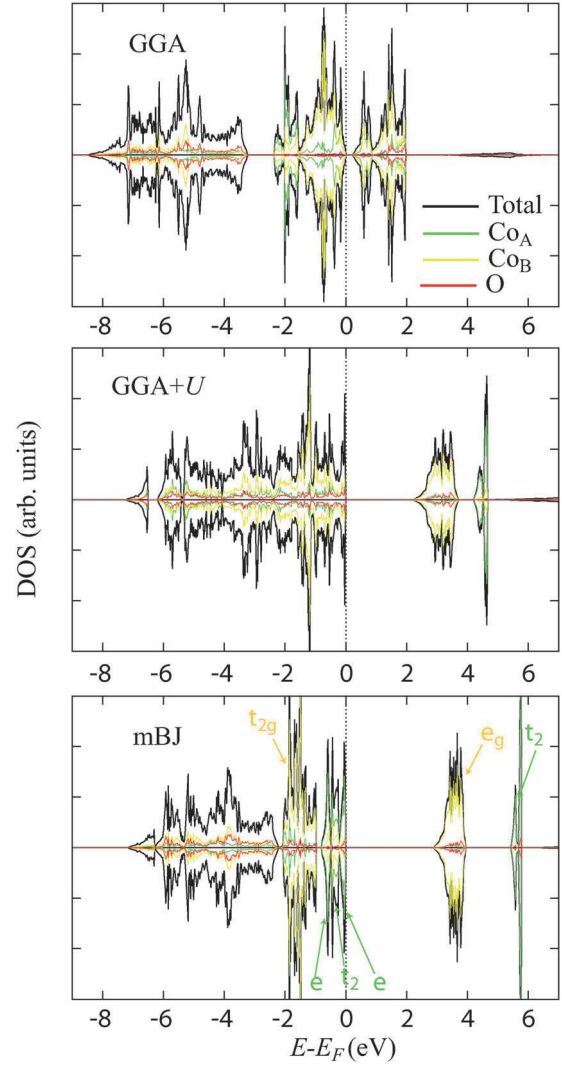


Fig. 1 Spin-resolved DOS for Co_3O_4 ($x = 0$) calculated using the 3 approximations.

coinciding with the atomic unit cell. From 33 K to 39 K, the magnetic ordering changes into an incommensurate spin structure, generally described as a spiral with a $[010]$ propagation vector. Below 33 K, the spin spiral becomes commensurate and the magnetic unit cell is doubled, with the resulting spin magnetic moments of the Mn_B atoms antiparallel in the $[010]$ direction to those of Mn_A . This magnetic phase below 33 K is closely linked to the atomic structure which can undergo a tetragonal-to-orthorhombic phase transition (from the space group $I4_1/amd$ to $Fddd$).^{55,56} Kemei *et al.*⁵⁶ have shown that both structural phases can coexist at low temperature. Strain effects can be envisaged to tune the magnetic properties⁵⁶ and the critical temperature.^{55,57}

An optical band gap of ≈ 2.4 eV was measured on thin films,^{58,59} while a higher value of 3.3 eV was reported on nanoparticles.⁶⁰ This shift of band gap was explained by a confinement effect. Hirai *et al.* reported absorption spectra from which they did not conclude about a band gap value. However, they found an absorption peak at ≈ 1 eV which can be

Table 1 Spin-resolved band gap energies ΔE and atomic spin magnetic moments M for different magnetic orderings. DOS from which the band gap energies were extracted are given in the ESI in Fig. 2S

| | $\Delta E(\uparrow)$ (eV) | $\Delta E(\downarrow)$ (eV) | $M(\text{Mn}_A)$ (μ_B per atom) | $M(\text{Mn}_B)$ (μ_B per atom) |
|--|---------------------------|-----------------------------|--------------------------------------|--------------------------------------|
| (a) Antiferromagnetic ($A^\uparrow[B^\uparrow, B^\downarrow]$): $M_{\text{tot}} = 0 \mu_B$, $a = 8.132 \text{ \AA}$, $c = 9.493 \text{ \AA}$ | | | | |
| GGA | 0.78 | 0.78 | ± 4.19 | ± 3.52 |
| GGA+ U | 1.37 | 1.37 | ± 4.53 | ± 3.84 |
| mBJ | 1.92 | 1.92 | ± 4.48 | ± 3.64 |
| (b) Ferrimagnetic ($A^\downarrow[B^\uparrow, B^\uparrow]$): $M_{\text{tot}} = 3 \mu_B$, $a = 8.107 \text{ \AA}$, $c = 9.610 \text{ \AA}$ | | | | |
| GGA | 0.78 | 0.52 | -4.13 | 3.48 |
| GGA+ U | 1.37 | 2.42 | -4.51 | 3.79 |
| mBJ | 2.40 | 1.42 | -4.44 | 3.56 |
| (c) Ferrimagnetic ($A^\uparrow[B^\downarrow, B^\uparrow]$): $M_{\text{tot}} = 5 \mu_B$, $a = 8.134 \text{ \AA}$, $c = 9.518 \text{ \AA}$ | | | | |
| GGA | 0.63 | 0.93 | 4.22 | ± 3.67 |
| GGA+ U | 1.17 | 1.79 | 4.53 | ± 3.84 |
| mBJ | 1.62 | 2.45 | 4.49 | ± 3.65 |
| (d) Ferromagnetic ($A^\uparrow[B^\uparrow, B^\uparrow]$): $M_{\text{tot}} = 13 \mu_B$, $a = 8.234 \text{ \AA}$, $c = 9.586 \text{ \AA}$ | | | | |
| GGA | 0.32 | 2.82 | 4.32 | 3.76 |
| GGA+ U | 0.78 | 4.00 | | |
| mBJ | 1.46 | 3.93 | 4.55 | 3.75 |
| (e) Experimental: $M_{\text{tot}} = 1.85\text{--}1.89 \mu_B$ ^{50,51,54} $a = 8.149 \text{ \AA}$, $c = 9.465 \text{ \AA}$ ¹² 2.4 ^{58,59} | | | | |
| | | | 4.64 ⁵¹ | 3.55 ⁵¹ |

consistent with the calculations of Franchini *et al.* who gave a band gap of 0.3–0.5 eV. They also found two optical band gaps of 1.9 eV and 4.0 eV (see the ESI of ref. 18).

We performed calculations with different magnetic orderings (antiferromagnetic, ferrimagnetic and ferromagnetic) and found that the antiferromagnetic configuration with a zero magnetic moment is the most stable. This result is consistent with the literature,^{15,18} and highlights a clear difference with a common ferrimagnetic ordering obtained due to a strong antiferromagnetic coupling between cations in B and A sites. In contrast, the spin magnetic moments per atom are in agreement with reported experimental measurements (see Table 1).¹²

The calculated DOS are displayed in Fig. 2. According to the mBJ calculations, the bands just below the Fermi level are built from the hybridization of dt_2 orbitals of Mn_A and d_{z^2} of Mn_B cations, and p orbitals of oxygen atoms, with, however, a noticeably higher contribution coming from the Mn_A ions, while the DOS presents mainly a d character from the Mn_B atoms for the GGA. The conduction bands with the lowest energy have a clear $\text{Mn}_B(d)$ symmetry no matter what the approximation is. According to the mBJ calculations, the top of the valence bands displays a main contribution coming from the $\text{Mn}_A(dt_2)$ orbitals, mixed with $\text{Mn}_B(d_{z^2})$ orbitals (the energy range of which extends from $E_F - 1.38 \text{ eV}$ to E_F), while the bottom of the conduction band has a clear $\text{Mn}_B(d_{x^2-y^2})$ character. We thus found a first band gap of 1.92 eV between the top of the valence band and the bottom of the conduction band, and the energy difference to the bottom of the unoccupied bands of the Mn_A atoms is 4.31 eV (also see the Fig. 3S, ESI[†]). These values are similar to those given by Hirai *et al.*¹⁸ which are $\simeq 1.43 \text{ eV}$ and $\simeq 3.41 \text{ eV}$ using DFT+ U , and 2.61 eV and 4.17 eV using the HSE06 hybrid functional.

Band gaps, magnetic moments and calculated lattice parameters are given in Table 1 for 4 magnetic configurations. The antiferromagnetic ordering brings the closest lattice parameters and band gaps (although lower by 20%), if compared with experimental measurements from the literature.^{58,59} However, the best fit for the total spin magnetic moment is obtained for the ferrimagnetic ordering with the $A^\downarrow[B^\uparrow, B^\uparrow]$ configuration. Although it does not correspond to the fundamental state, the band gap energy calculated for the majority spin electrons is still in agreement with values reported in the literature. For an easier understanding, the last case will be used as a reference in the next section.

3.3 $\text{Mn}_x\text{Co}_{3-x}\text{O}_4$

For our calculations, we considered 13 different supercells with a varying number x of Mn atoms substituted for Co in Co_3O_4 . We first considered the substitution as occurring in the B sites, and then, once every Co_B was replaced by Mn atoms (for $x = 2.0$), every added Mn was set into the A sites, in accordance with neutron diffraction measurements, Rietveld refinements and bond valence sum calculations reported in ref. 12. Apart from Co_3O_4 , for which we considered an initial antiferromagnetic ordering, all the other calculations were performed using a ferrimagnetic arrangement with antiparallel alignment of spin magnetic moments of cations in A sites compared with those in B sites (*i.e.* $A^\downarrow[B^\uparrow, B^\uparrow]$). The last choice will be justified in Section 3.3.2.

3.3.1 Atomic structures. The complete set of lattice parameters was calculated for all $\text{Mn}_x\text{Co}_{3-x}\text{O}_4$ compounds using the GGA approximation. The results are displayed in Fig. 3 and compared with experimental data obtained by X-ray diffraction measurements on single phase sintered ceramics.¹² For the cell volume, calculated and experimental data are in agreement for

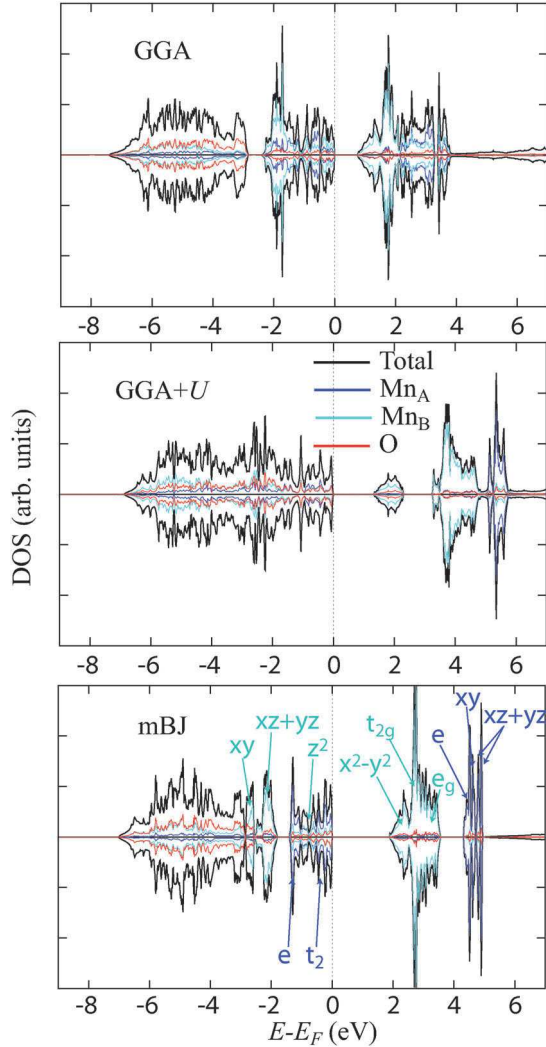


Fig. 2 Spin-resolved DOS for Mn_3O_4 ($x = 3.0$) calculated using the 3 approximations and for an antiferromagnetic ordering.

the extremum compositions (*i.e.* $x = 0-0.25$ and $x = 3$). The volume increases almost linearly as a function of x (the average increase of the volume is 34 \AA^3 per added Mn atom per f.u.) and the calculated values only underestimate the experimental values by at most 2.4% for intermediate compositions.

Considering the lattice parameters, some discrepancies appear more clearly. For $x < 2.0$, the three calculated lattice

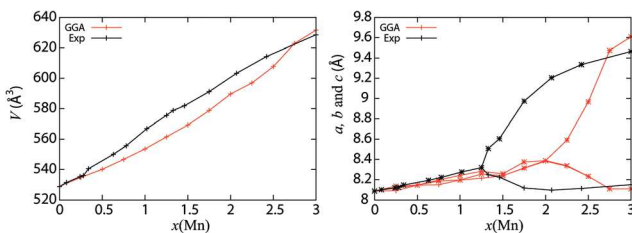


Fig. 3 Calculated volume V and lattice parameters a (+), b (\times) and c (\ast) compared to the experimental values of ref. 12. The results are given for a conventional cubic or tetragonal cell of 8 $\text{Mn}_x\text{Co}_{3-x}\text{O}_4$ formula units.

parameters are very close, while the chosen cationic distribution can artificially break apart the symmetries, the lattice can be considered as cubic in this range of x values. The calculations predict a cubic ($a = b = c$) to tetragonal ($c > a = b$) transition from $x > 2.0$, *i.e.* when all the occupied B sites are filled by Mn atoms and all the added atoms are thus placed into the A sites. If the transition was demonstrated to be correct, the critical composition at which it occurs is not consistent with the experiment: this transition has indeed been measured to occur from $x > 1.25$, and has been attributed to the presence of a sufficient amount ($\geq 55\%$ of the occupied B sites, *i.e.* for $x > 1.25^{12,61}$) of Mn_B^{3+} , with a d^4s^0 electronic structure, inducing a Jahn–Teller distortion. It is thus surprising that Mn_2CoO_4 (for which 100% of the B sites are occupied by Mn atoms) is still found to be cubic by the calculations.

Because the transition only begins when additional Mn atoms replace Co atoms in the A site, we verified that, besides the Jahn–Teller effect, the presence of Mn atoms in these A sites could not provide a complementary explanation. A calculation was then performed for $x = 1.0$, and with 1/4 of the Mn atoms swapped with the cobalt in the A sites. Again, a cubic structure was found, with a volume only slightly reduced by 1% in comparison with the ideal case in which all the Mn atoms were in the B sites. According to these results, we can thus conclude that the presence of Mn_A sites is not the reason for the tetragonal distortion. In addition, the total energy calculated for the structure with the swap defect was found to be 0.45 eV higher than that for the ideal structure, which confirms the experimental cation distribution with a preferential location of Mn atoms in B sites.

The inability of GGA calculations to correctly reproduce the tetragonal shape of the lattice between $1.25 < x \leq 2.0$ can originate from the wrong description of the magnetism to which it is known to be intimately related, as discussed before in the case of Mn_3O_4 .^{55,56} The calculations only predict the cubic-to-tetragonal transition to happen when a critical value of the volume is reached due to a cell increase produced by the addition of Mn atoms in either A or B sites. The influence of the temperature should also be taken into account, as the current experimental data have been obtained at room temperature, whereas magnetic phases under consideration, as well as our calculations, are only considered at low temperatures. These different aspects could explain the limit value of x calculated for the transition.

Finally, we would like to mention that the GGA+ U method has also been tried for the calculations of the lattice parameters, but we did not retain the results as they worsen the comparison with our experimental measurement. In that case, the shape of the structures was completely different and the volume tends to be overestimated (see Fig. 4S, ESI[†]). Other studies have already underlined the possibility of stabilising tetragonal or orthorhombic manganite spinel lattices by using different approximations.⁶²

3.3.2 Magnetic properties. For the lowest non-zero concentration of Mn atoms ($x = 0.25$), the antiferromagnetic coupling between Co_A and Mn_B is sufficient to set up the ferrimagnetic

ordering. We indeed mapped different magnetic ordering and found that this composition displays the lowest total energy. Moreover, we have checked that this ferrimagnetic ordering remains robust for high x values, *i.e.* $x = 2.0$ and 2.5 , by comparing the total energy for the different magnetic states, similarly to the calculations done for Mn_3O_4 . The obtained ferrimagnetic state is in agreement with experimental measurements,^{14,49,63} and also with recently published theoretical results obtained on similar compounds $\text{Ni}_x\text{Co}_{3-x}\text{O}_4$.⁶⁴

As shown in Fig. 4a and following the GGA calculations, the Co_B atoms merely present a low-spin state. From $x > 0.5$, these atoms begin however to be spin-polarized and adopt an intermediate spin state due to the presence of surrounding Mn_B atoms. The increase of the magnetic moments of Co_B is also consistent with an increase of the content and the spin moment of the Mn_B atoms. Such a change in the magnetic moments can result from a charge reorganization at the orbital level inside each atom separately, due to their mutual influence, but can also be due to a charge transfer from Mn^{3+} to Co^{III} cations, with an increase and a decrease of the d-orbital occupancy, respectively, in agreement with experimental hypothesis given in several references.^{13,63,65} For the mBJ calculations, performed using the GGA, the most stable initial magnetic configuration, the Co_B atoms present strictly a low spin state, with no spin-polarization, in the $0 \leq x < 2.0$ range. The magnetic moments of the different atoms remain approximately constant. In contrast, using the GGA+ U method, the spin-polarization of the Co_B is more pronounced than using the GGA and the Co_B directly switches from the low-spin to the high-spin configuration for $x > 0.5$. This result certainly strongly depends on the relative strength of the electronic correlations, *i.e.* on the chosen value of the U_{eff} parameter, with respect to the crystal field splitting. On the other hand, it is also important to keep in mind that the crystal field effect is directly related to the structure and can be enhanced by the tetragonal distortion of the lattice, which is not correctly taken into account in our calculations, for $1.25 \leq x \leq 2.0$.

The experimental absolute value of the averaged magnetic moments per atomic site reported in Fig. 4b were determined at 10 K by the neutron diffraction technique.¹⁴ A complex behavior is emphasized, being not correctly reproduced by our calculations, in particular for the GGA and mBJ calculations. The low magnetic moment at $x = 0.25$ tends to suggest that the Co_B atoms are still in a low- or intermediate-spin state, and that the Co_A moments are still arranged in a configuration close to the antiferromagnetic ordering. The ferrimagnetism (ferromagnetic alignment of the Co_A magnetic moments) is then set from $x = 0.75$, that is at a higher value of x than that found by the calculations, and the Co_B atoms seem to switch to a high-spin state, in agreement with the GGA+ U results. Then, the lowering of the magnetic moments for both types of cations at $x = 1.25$ is certainly due to the sufficiently high number of Mn atoms which induce a non-collinear ordering involving the B sublattice.

The calculated variation of the absolute value of the total magnetic moment is shown in Fig. 4c. According to the GGA calculations, from $x = 0.25$ to 0.75 , the direction of the total spin

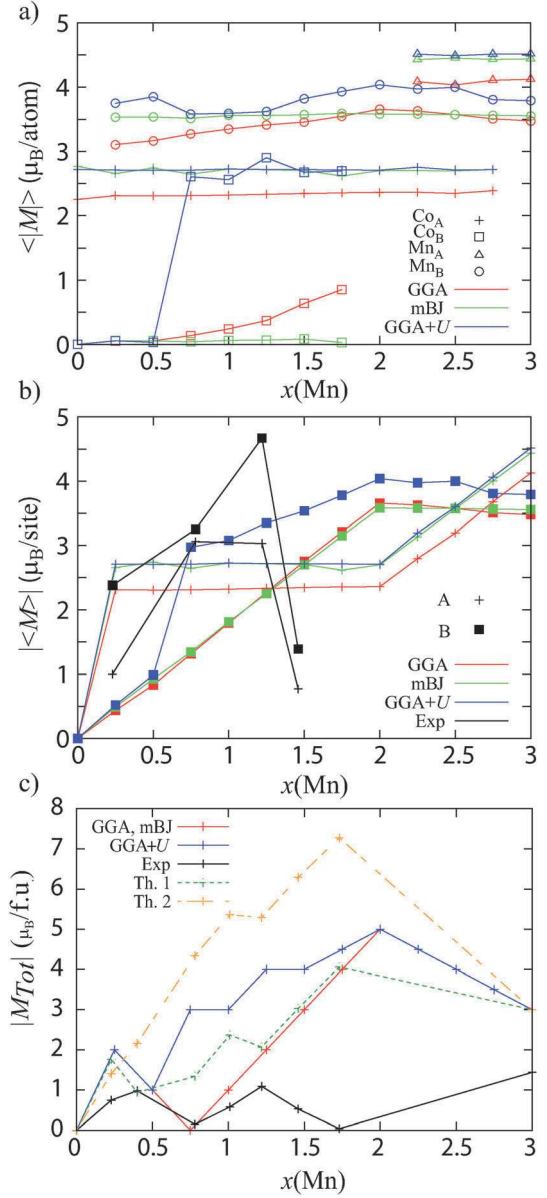


Fig. 4 Variation of the spin magnetic moments as a function of the Mn concentration x in $\text{Mn}_x\text{Co}_{3-x}\text{O}_4$: (a) average of the absolute value per atom and per atomic site, (b) absolute value of the average ($\text{Co} + \text{Mn}$ atoms) per atomic site, and (c) absolute value of the total magnetic moment per f.u. The experimental values are taken from ref. 14.

magnetic moment is governed by the magnetic moments of the Co_A and its value increases by $1 \mu_B$ when x increases by 0.25 . For $x = 0.75$, the sum of the magnetic moments of the Co_A is exactly equal to the sum of those for the Mn_B atoms (with an opposite sign), which corresponds to a total magnetic moment of $0 \mu_B$ and to an inversion of its direction. For $x > 0.75$, the orientation of the total magnetic moment is then the same as the magnetic moments of the Mn_B cations. A progressive magnetic moment increase is observed until $x = 2.0$, when added Mn^{2+} cations replace Co_A^{2+} , which have a lower magnetic moment, thus inducing a decrease of the total magnetic moment of $0.5 \mu_B$ per $x = 0.25$. The total magnetic moment calculated using the

GGA+ U adopts a higher value than using the GGA calculations for x varying from 0.5 to 1.75 due to the low-spin to high-spin transition.

The magnetization measurements described in Fig. 4c (black curve) were performed at 5 K,¹⁴ well under the ordering temperature, in agreement with very early studies.^{49,66} The curve displays a similar behavior to that for the GGA and mBJ calculations for $x < 1.25$, even if the total magnetic moment value is significantly lower. Then we observed a decrease of the absolute value of the magnetization that takes place simultaneously with the experimentally observed tetragonal distortion of the lattice, for $x = 1.25$. No jump of the magnetization value, indicative of a low spin to high spin transition, is observed in this range of compositions.

We also plotted two curves in Fig. 4c that correspond to the theoretical magnetic moment variations (called Th.1 and Th.2) assuming a collinear magnetic model, that all the Co_B are in a low-spin state (Th.1) or in an averaged state between the low and the high spins (Th.2), and taking into account the oxidation degrees measured from ref. 12 and 67. GGA+ U calculations display a similar tendency as the curves Th.1 and Th.2, but with an absolute value of the total magnetic moment intermediate between that of the two curves. The GGA calculations and the experimental measurements are however clearly different around $x = 0.75$. We can suggest from these observations that the presence of Co_B ions with a magnetic moment different from 0, due to a different oxidation degree or due to the transition toward an intermediate or a high-spin state, is not so obvious, particularly if we consider that, in experimental measurements, the change of the magnetization due to these processes could compete with variations due to the non-collinear magnetic ordering.

The overall lower measured magnetization, in comparison with theoretical values, can be either attributed to structural defects, which cannot be avoided in such materials (antiphase boundaries, vacancies, interstitials, Frenkel pairs), to size

effects, and/or to deviations from the collinear magnetic ordering. Indeed, the moment decrease observed at $x = 1.25$ (and not reproduced by any of the theoretical models or calculations) can be due to a transition because of the large number of Mn_B cations that can induce a new and more complex magnetic ordering, similar to pure Mn_3O_4 . Moreover, such magnetic transition is concomitant with the experimental tetragonal distortion.

For the different reasons discussed previously, we performed some calculations with the lattice parameters measured experimentally.¹² For $x = 2.0$ and 2.5, we verified that the ferrimagnetic ordering was still the most stable magnetic state, using both the GGA and GGA+ U approximations. For $x = 1.75$, the Co_B atoms are also still in low-spin states according to the GGA, and have their moment only decreased by 7.5%, compared to the calculated values with the cubic structure. The variations of the magnetic moments are even smaller in the case of the other atoms (by at most 3%) and the total magnetic moment remains exactly the same, which means that the magnetization decreases proportionally to the slightly larger measured volume.

Therefore, our calculations provided some results which remain stable with a reliable change in volume and lattice constants.

3.3.3 Electronic structures. To illustrate the electronic structure obtained for the $\text{Mn}_x\text{Co}_{3-x}\text{O}_4$ materials, two sets of DOS calculated using the three approximations described earlier are shown in Fig. 5, for $x = 1$ and 2.5, *i.e.* for the B and A sites filled by an equal amount of Co and Mn atoms, respectively (also see the complete set of DOS in Fig. 5S–8S of the ESI[†]). As for pure Co_3O_4 and Mn_3O_4 , the GGA+ U approximation increases the band gap around the Fermi energy, compared to the GGA calculations, by shifting the d band energies of the cations, which inevitably induces more overlapping between the cation and oxygen orbitals (originally lying at lower energy) and increases the cation–anion and cation–cation hybridizations. In contrast, the mBJ calculations result in a net separation of the d bands of the cations and the p bands of oxygen. This is consistent with the fact that Co_B does not spin polarize under the magnetic influence of the Mn atoms and that every magnetic moment remains constant as a function of x . This result is also in agreement with a constant oxidation degree for each cation, *i.e.* $\text{Co}_A^{2+}(\text{d}^7\text{s}^0)$, $\text{Mn}_A^{2+}(\text{d}^5\text{s}^0)$, $\text{Co}_B^{\text{III}}(\text{d}^6\text{s}^0)$ and $\text{Mn}_B^{3+}(\text{d}^4\text{s}^0)$.

All calculations show a strong decrease of the fundamental band gap compared to the two end members Co_3O_4 and Mn_3O_4 , with a more pronounced effect for the GGA and GGA+ U approximations that tend to describe a half-metallic character of any $\text{Mn}_x\text{Co}_{3-x}\text{O}_4$ compounds for $0.25 \leq x \leq 2.5$ (see Fig. 9S of the ESI[†]). Similar results have been reported on $\text{Ni}_x\text{Co}_{3-x}\text{O}_4$ by Shi *et al.*⁶⁴ The non-zero DOS at the Fermi level could be indicative of the simultaneous presence of Mn^{3+} and Mn^{4+} in the B sites and of the conductivity setting by a double-exchange mechanism.

The complete variation of the electronic structure investigated in mBJ as a function of the composition is given in Fig. 6, with a schematic representation of the main atomic contributions to the electronic structure (Fig. 6a). The up and down directions for the spin of the electrons are defined by the up and down arrows (\uparrow, \downarrow) respectively, which can either correspond to minority or majority spin directions, depending on the x concentration of Mn ions. For an easier comparison of the electronic structure evolution, the magnetic moments of the B-site atoms are always chosen parallel to \uparrow , while the magnetic moments of A atoms are parallel to \downarrow , and therefore the total magnetic moment will then be parallel to the \downarrow direction for $0 < x < 0.75$ and to the \uparrow direction for $0.75 < x < 3.0$. The fundamental band gap calculated using this approximation corresponds to the energy separation between the occupied and unoccupied e_g bands (d_{z^2} and $\text{d}_{x^2-y^2}$, respectively) of Mn_B atoms, for $0.25 \leq x \leq 3$. Therefore, introducing a small fraction of Mn in Co_3O_4 will directly induce a large decrease of the band gap value (of 73% from $x = 0$ to $x = 0.25$ according to the mBJ calculations), by strongly lowering the occupied d-band energies of the Co atoms for the \uparrow -spin configuration. Between $x = 0.25$ and $x = 2$, the band gap, calculated using the mBJ method, varies from $\simeq 0.2$ to 0.8 eV. The band gap then increases almost linearly from $x = 2$ to 3, when the tetragonal distortion is set. According to the mBJ calculated band gap, only a small excitation energy

would be necessary to activate conductivity processes *via* electron hopping.

Occupied d-bands of the Co_A atoms for the \uparrow -spin configuration are located between the e_g bands of the Mn_B atoms and the t_{2g} bands of the Co_B or Mn_B . This can be associated with the presence of intermediate bands as suggested in the literature.^{11,19} However, we find that only the e_g bands of the Mn_B strongly contribute to the band gap width.

The energy differences ΔE between the top of the occupied bands (composed of O-p, $[\text{Mn}, \text{Co}]_A$ -d or $[\text{Mn}, \text{Co}]_B$ -d) and the bottom of the unoccupied bands (composed of $[\text{Mn}, \text{Co}]_A$ -d or $[\text{Mn}, \text{Co}]_B$ -d) are detailed in Fig. 6b. All these data have been directly extracted from the DOS (ESI[†]).

The two sets of experimental optical band gaps measured by Salek and some of the current authors,¹¹ reported in Fig. 6b for comparison with our calculated values, should then correspond to transitions between d bands of cations in A sites toward

cations in B sites ($A \rightarrow B$ with green curve) for the lowest experimental values, and from B sites to B sites ($B \rightarrow B$ with the yellow curve) for the highest values, all with the \uparrow -spin, although the highest band gap corresponding to the absorption peak in the UV-visible region is usually admitted to be related to $O \rightarrow B$ transitions. Transition from A to B sites for the minority spin between $x = 1.5$ and $x = 2.5$ is also in the good range of energies. It is also important to note that the fundamental band gap (corresponding, for each compound, to the lowest value between the $B \rightarrow B$ transition with the blue curve in the top panel of Fig. 6b, and the $A \rightarrow B$ green curve of the bottom panel) is still much lower than the energy gap values determined experimentally, which can be explained by the fact that such an energy range is not usually explored experimentally. For a very low value of x , we can also expect that the electronic states of the Mn_B atoms are too localized to be mapped experimentally.

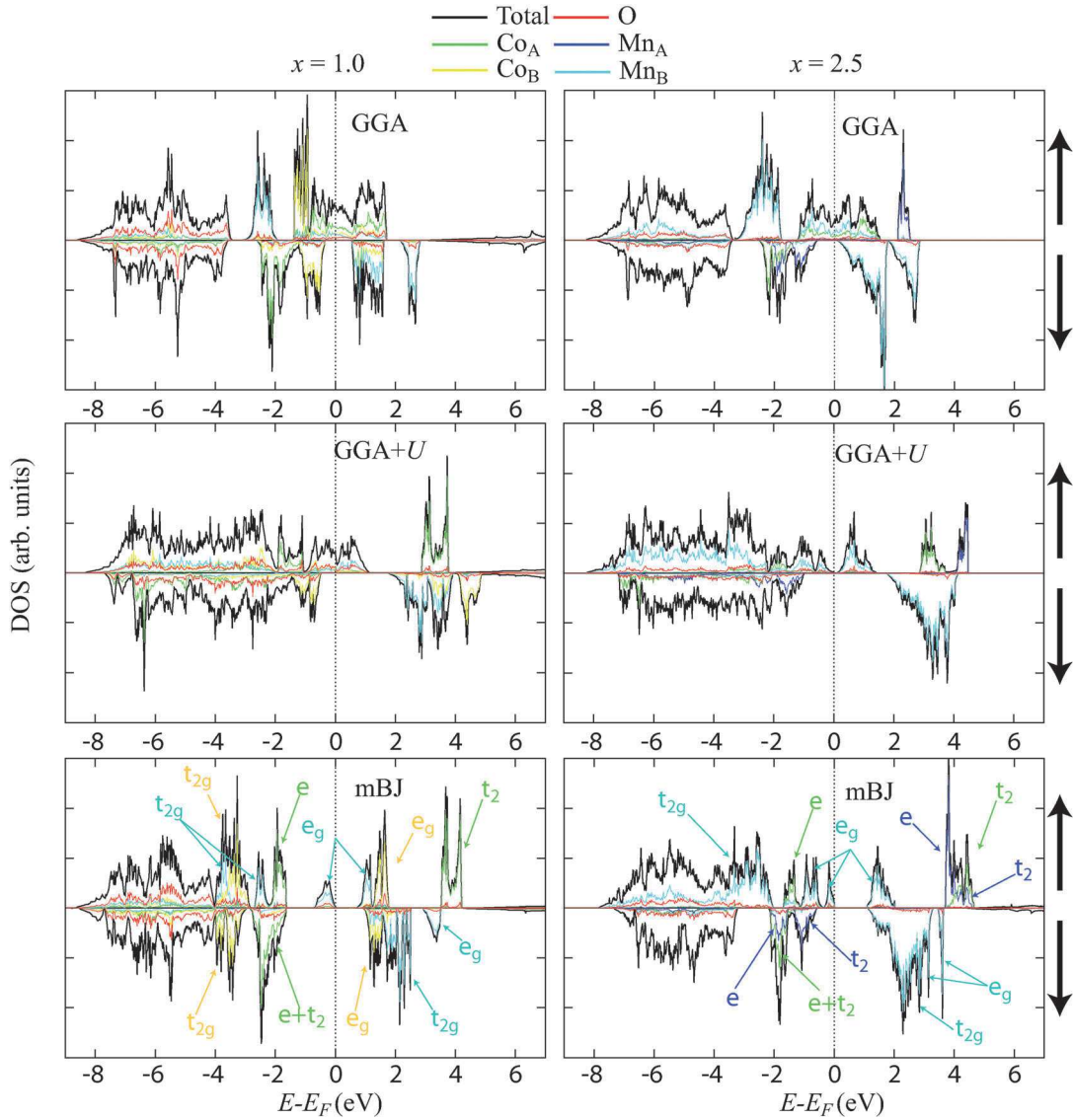


Fig. 5 Spin-resolved DOS for the MnCo_2O_4 (left) and $\text{Mn}_{2.5}\text{Co}_{0.5}\text{O}_4$ (right) determined by GGA, GGA+ U and mBJ calculations.

Finally, ΔE values corresponding to possible electronic transitions in the $1.5 \leq x \leq 2.5$ range, obtained from electronic structure calculations performed by using the experimental lattice parameters,¹² *i.e.* with a higher tetragonal distortion, are shown in Fig. 6c. These data clearly show that the tetragonal distortion of the lattice, related to the Jahn-Teller effect, induces a significant increase of the band gap values, while they still remain lower than the measured experimental values. Such an increase is similar to the one determined using the

calculated lattice parameters, for $2 \leq x \leq 3$, and goes along with a small shift toward higher energies of the bands, which are the closest from the Fermi level, for the majority spin electrons. Using the calculated lattice parameters allows us to remain in a full *ab initio* configuration for our calculations, but in that case, the results obtained using the experimental lattice parameters are certainly more reliable. A comparison between the two sets of calculations is however interesting as it gives some clues on how the electronic structure, and thus the

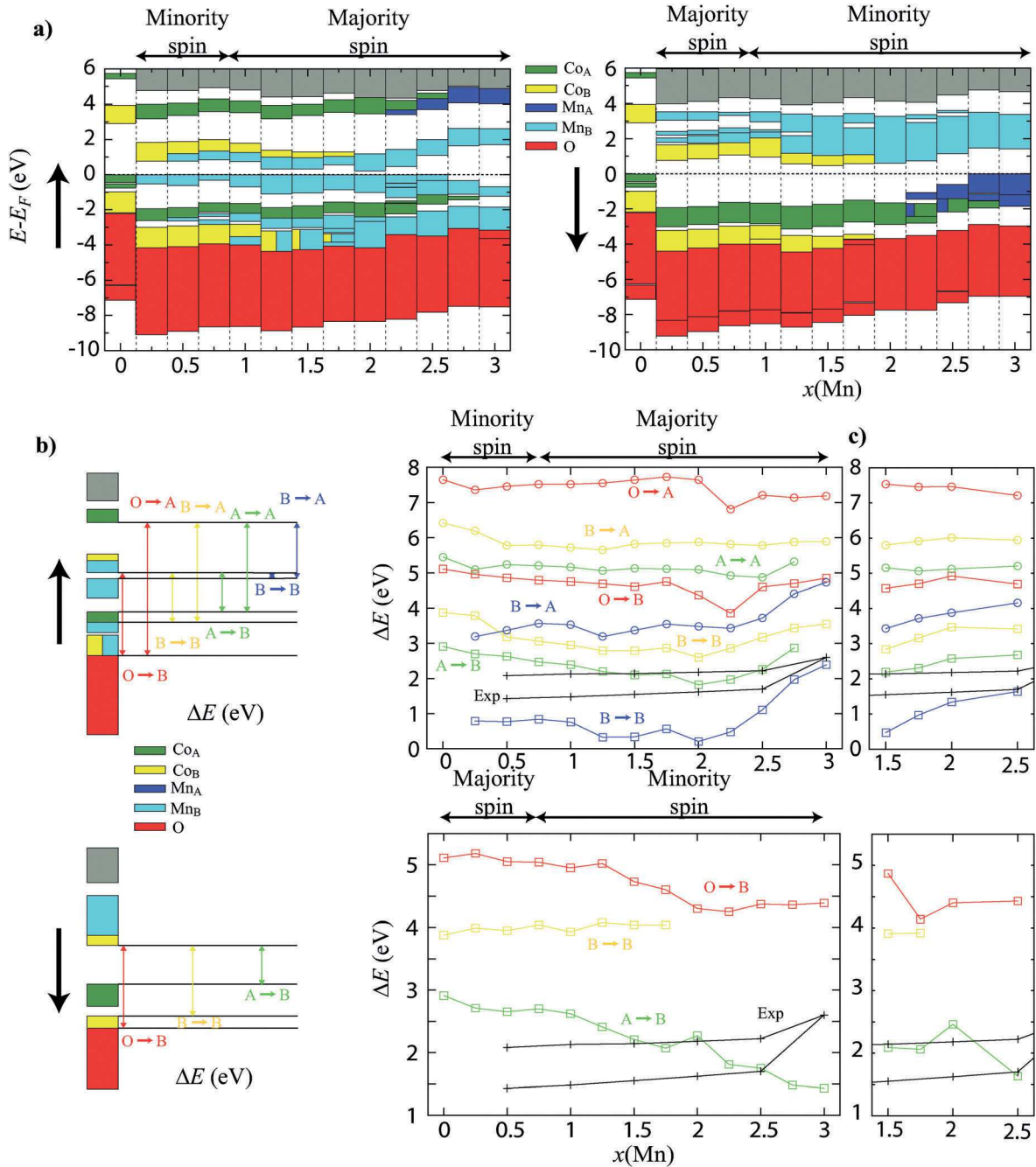


Fig. 6 (a) Schematic representation of the band distributions as calculated using the mBJ approximation for a ferrimagnetic ordering (except for antiferromagnetic Co_3O_4). (b) Calculated energy differences ΔE , which may correspond to optical transition, as a function of x and obtained using calculated lattice parameters (experimental data are taken from ref. 11 and 68), and (c) using the experimental tetragonal lattice parameters.

photoelectric properties, could change and be tuned by inducing some strain on the lattice.

4 Conclusion

The electronic band structure, cell parameters and magnetic characteristics of $\text{Mn}_x\text{Co}_{3-x}\text{O}_4$ ($0 \leq x \leq 3$) were determined for the first time over the whole solid solution range thanks to *ab initio* DFT-based calculations and compared with experimental data.

Our results are in accordance with those reported in the literature for the pure end member compounds Co_3O_4 ($x = 0$) and Mn_3O_4 ($x = 3$). The main properties of the antiferromagnetic Co_3O_4 are quite well reproduced even if an uncertainty can remain regarding the band gap value which could be lower (≈ 0.8 eV) than that we calculated using the mBJ calculations (≈ 2.91 eV). The case of Mn_3O_4 is more complicated as this compound displays a complex ferrimagnetic ordering at low temperature, which can be approximated using collinear-magnetism calculations for different magnetic states with a close total energy. We found that the most stable solution corresponds to a full antiferromagnetic ordering, with a band gap of 1.92 eV.

The interpretation of the calculated results, which strongly depends on the used methods and parameters, can be harder for the intermediate compounds ($0 < x < 3$), due to the complexity of the cation distribution and oxidation states possible for the cubic and tetragonal phases. However, our calculations give a cubic-to-tetragonal distortion of the lattice while increasing x . This transition is however predicted at $x > 2.0$, instead of $x > 1.25$ from the experimental data, which is not consistent with the usual Jahn–Teller effect description. Several inter-correlated contributions can be suggested to explain such a difference, as a lower calculated volume and a wrong description of the electron correlation effects or a complex non-collinear magnetic ordering.

All intermediate compositional materials are ferrimagnetic at low temperature, with cations in A sites having spin magnetic moments antiparallel to those in B sites, in agreement with experimental studies. However, this ferrimagnetic ordering is certainly non-collinear, and might become more complicated to describe as the Mn content increases in B sites. In addition, the potential presence of structural defects could partly explain the lower experimental magnetization and its decrease measured for $x \geq 1.25$. Co_B^{III} cations are always found in a low-spin state for $0 \leq x < 2.0$ using the mBJ calculations, while the GGA+U method predicts a transition toward a high-spin state for $x > 0.5$. For $1.5 \leq x \leq 2.5$, our calculations showed that the magnetic properties were not affected by a change in the crystal shape. Monte-Carlo calculations could be envisaged in order to take into account the highly complex magnetic ordering, as well as the temperature effect, and shall be conducted for the ordering temperature determination.

The electronic and band structures of the cobalt and manganese spinel oxide materials were also determined. The band gap is strongly decreased upon doping of the pure end members of

the Mn_3O_4 – Co_3O_4 spinel family, which can be explained by the lowest band gap always found between the split e_g bands (d_{z^2} for the occupied band and $d_{x^2-y^2}$ for the unoccupied bands). Such a band gap is barely mentioned in the literature based on experimental studies, but mainly because of the restricted measurement range areas. It is supposed to have a value of ~ 0.5 eV for the cubic phase, and a higher value, up to ~ 1.5 eV, for the tetragonal phase. This transition would be related to cation–cation transitions with an “up”-spin direction in octahedral sites. The band gap width for the intermediate compounds is thus mainly governed by the shape of the lattice (cubic *versus* tetragonal). The photoelectric properties of such materials could then be tuned by controlling strain effects in the lattice.

Acknowledgements

This work was granted access to the HPC resources of the CALMIP supercomputing center under the allocation p1313 (2014–2016).

References

- 1 B. Kupfer, K. Majhi, D. A. Keller, Y. Bouhadana, S. Rühle, H. N. Barad, A. Y. Anderson and A. Zaban, *Adv. Energy Mater.*, 2015, 5, 1401007.
- 2 M. Long, W. Cai, J. Cai, B. Zhou, X. Chai and Y. Wu, *J. Phys. Chem. B*, 2006, 110, 20211.
- 3 A. K. Chakraborty, M. S. Akter, M. A. Haque and M. S. A. G. M. A. Khan, *J. Cluster Sci.*, 2013, 24, 701.
- 4 N. Bahlawane, E. F. Rivera, K. Kohse-Hoinghaus, A. Brechling and U. Kleineberg, *Appl. Catal., B*, 2004, 53, 245.
- 5 L. Qiao, H. Y. Xiao, H. M. Meyer, J. N. Sun, C. M. Rouleau, A. A. Puretzky, D. B. Geohegan, I. N. Ivanov, M. Yoon, W. J. Weber and M. D. Biegalski, *J. Mater. Chem. C*, 2013, 1, 4628.
- 6 K. J. Kormondy, A. B. Posadas, A. Slepko, A. Dhamdhare, D. J. Smith, K. N. Mitchell, T. I. Willett-Gies, S. Zollner, L. G. Marshall, J. Zhou and A. A. Demkov, *J. Appl. Phys.*, 2014, 115, 243708.
- 7 L. Ren, S. Wu, W. Zhou and S. Li, *J. Cryst. Growth*, 2014, 389, 55.
- 8 A. Matsuda, R. Yamauchi, D. Shiojiri, G. Tan, S. Kaneko and M. Yoshimoto, *Appl. Surf. Sci.*, 2015, 349, 78.
- 9 S. Apelt, Y. Zhang, J. Zhu and C. Leyens, *Surf. Coat. Technol.*, 2015, 280, 208.
- 10 R. N. Singh, J. P. Pandey, N. K. Singh, B. Lal, P. Chartier and J.-F. Koenig, *Electrochim. Acta*, 2000, 45, 1911.
- 11 G. Salek, P. Dufour, S. Guillemet-Fritsch and C. Tenailleau, *Mater. Chem. Phys.*, 2015, 162, 252.
- 12 H. Bordeneuve, C. Tenailleau, S. Guillemet-Fritsch, R. Smith, E. Suard and A. Rousset, *Solid State Sci.*, 2010, 12, 379.
- 13 A. Rousset, C. Tenailleau, P. Dufour, H. Bordeneuve, I. Pasquet, S. Guillemet-Fritsch, V. Poulain and S. Schuurman, *Int. J. Appl. Ceram. Technol.*, 2013, 10, 175.
- 14 S. Guillemet-Fritsch, C. Tenailleau, H. Bordeneuve and A. Rousset, *Adv. Sci. Technol.*, 2010, 67, 143.

- 15 A. Chartier, P. D'Arco, R. Dovesi and V. R. Saunders, *Phys. Rev. B: Condens. Matter Mater. Phys.*, 1999, **60**, 14042.
- 16 C. Franchini, R. Podloucky, J. Paier, M. Marsman and G. Kresse, *Phys. Rev. B: Condens. Matter Mater. Phys.*, 2007, **75**, 195128.
- 17 R. Kaur, T. Maitra and T. Nautiyal, *AIP Conf. Proc.*, 2004, **1591**, 1137.
- 18 S. Hirai, Y. Goto, Y. Sakai, A. Wakatsuki, Y. Kamihara and M. Matoba, *J. Phys. Soc. Jpn.*, 2015, **84**, 114702.
- 19 S. Thota, A. Kumar and J. Kumar, *J. Mater. Sci. Eng. B*, 2009, **164**, 30.
- 20 J. Chen, X. Wu and A. Selloni, *Phys. Rev. B: Condens. Matter Mater. Phys.*, 2011, **83**, 245204.
- 21 A. Lima, *J. Phys. Chem. Solids*, 2014, **75**, 148.
- 22 V. Singh, M. Kosa, K. Majhi and D. T. Major, *J. Chem. Theory Comput.*, 2016, **11**, 64.
- 23 V. Singh and D. T. Major, *Inorg. Chem.*, 2016, **55**, 3307.
- 24 X.-L. Xu, Z.-H. Chen, Y. Li, W.-K. Chen and J.-Q. Li, *Surf. Sci.*, 2009, **603**, 653.
- 25 X.-Y. Pang, C. Liu, D.-C. Li, C.-Q. Lv and G.-C. Wang, *ChemPhysChem*, 2013, **14**, 204.
- 26 J. Chen and A. Selloni, *Phys. Rev. B: Condens. Matter Mater. Phys.*, 2012, **85**, 085306.
- 27 C.-Q. Lv, C. Liu and G.-C. Wang, *Catal. Commun.*, 2014, **45**, 83.
- 28 P. S. Arun, B. Ranjith and S. M. A. Shibli, *Environ. Sci. Technol.*, 2013, **47**, 2746.
- 29 F. Zasada, J. Grybos, P. Indyka, W. Piskorz, J. Kaczmarczyk and Z. Sojka, *J. Phys. Chem. C*, 2014, **118**, 19085.
- 30 Y. Li, M. Wu and C. Ouyang, *Appl. Surf. Sci.*, 2015, **349**, 510.
- 31 P. E. Blöchl, *Phys. Rev. B: Condens. Matter Mater. Phys.*, 1994, **50**, 17953.
- 32 G. Kresse and J. Hafner, *Phys. Rev. B: Condens. Matter Mater. Phys.*, 1994, **49**, 14251.
- 33 G. Kresse and J. Furthmüller, *Phys. Rev. B: Condens. Matter Mater. Phys.*, 1996, **54**, 11169.
- 34 H. J. Monkhorst and J. D. Pack, *Phys. Rev. B: Condens. Matter Mater. Phys.*, 1976, **13**, 5188.
- 35 J. P. Perdew, K. Burke and M. Ernzerhof, *Phys. Rev. Lett.*, 1996, **77**, 3865.
- 36 A. D. Becke and E. R. Johnson, *J. Chem. Phys.*, 2006, **124**, 221101.
- 37 F. Tran and P. Blaha, *Phys. Rev. Lett.*, 2009, **102**, 226401.
- 38 V. I. Anisimov, I. V. Solovyev, M. A. Korotin, M. T. Czyżyk and G. A. Sawatzky, *Phys. Rev. B: Condens. Matter Mater. Phys.*, 1993, **48**, 16929.
- 39 S. L. Dudarev, G. A. Botton, S. Y. Savrasov, C. J. Humphreys and A. P. Sutton, *Phys. Rev. B: Condens. Matter Mater. Phys.*, 1998, **57**, 1505.
- 40 D. Koller, F. Tran and P. Blaha, *Phys. Rev. B: Condens. Matter Mater. Phys.*, 2011, **83**, 195134.
- 41 W. L. Roth, *J. Phys.*, 1964, **25**, 507.
- 42 W. L. Roth, *J. Phys. Chem. Solids*, 1964, **25**, 1.
- 43 K. J. Kim and Y. R. Park, *Solid State Commun.*, 2003, **127**, 25.
- 44 X. Wang, X. Chen, L. Gao, H. Zheng, Z. Zhang and Y. Qian, *J. Phys. Chem. B*, 2004, **108**, 16401.
- 45 P. H. T. Ngamou and N. Bahlawane, *Chem. Mater.*, 2010, **22**, 4158.
- 46 A. Gasparotto, D. Barreca, D. Bekermann, A. Devi, R. A. Fischer, P. Fornasiero, V. Gombac, O. I. Lebedev, C. Maccato, T. Montini, G. V. Tendeloo and E. Tondello, *J. Am. Chem. Soc.*, 2011, **133**, 19362.
- 47 W. E. Pickett, S. C. Erwin and E. C. Ethridge, *Phys. Rev. B: Condens. Matter Mater. Phys.*, 1998, **58**, 1201.
- 48 V. Baron, J. Gutzmer, H. Rundlöf and R. Tellgren, *Am. Mineral.*, 1998, **83**, 786.
- 49 B. Boucher, R. Buhl, R. D. Bella and M. Perrin, *J. Phys.*, 1970, **31**, 113.
- 50 K. Dwight and N. Menyuk, *Phys. Rev.*, 1960, **119**, 1470.
- 51 B. Boucher, R. Buhl and M. Perrin, *J. Phys. Chem. Solids*, 1971, **32**, 2429.
- 52 G. B. Jensen and V. Nielsen, *J. Phys. C: Solid State Phys.*, 1974, **7**, 409.
- 53 G. Srinivasan and M. S. Seehra, *Phys. Rev. B: Condens. Matter Mater. Phys.*, 1983, **28**, 1.
- 54 B. Chardon and F. Vigneron, *J. Magn. Magn. Mater.*, 1986, **58**, 128.
- 55 M. Kim, X. M. Chen, X. Wang, C. S. Nelson, R. Budakian, P. Abbamonte and S. L. Cooper, *Phys. Rev. B: Condens. Matter Mater. Phys.*, 2011, **84**, 174424.
- 56 M. C. Kemei, J. K. Harada, R. Seshadri and M. R. Suchomel, *Phys. Rev. B: Condens. Matter Mater. Phys.*, 2014, **90**, 064418.
- 57 L. Ren, S. Wu, M. Yang, W. Zhou and S. Li, *J. Appl. Phys.*, 2013, **114**, 053907.
- 58 H. Y. Xu, S. L. Xu, X. D. Li, H. Wang and H. Yan, *Appl. Surf. Sci.*, 2006, **252**, 4091.
- 59 D. P. Dubal, D. S. Dhawale, R. R. Salunkhe, S. M. Pawar and C. D. Lokhande, *Appl. Surf. Sci.*, 2010, **256**, 4411.
- 60 N. M. Hosny and A. Dahshan, *Mater. Chem. Phys.*, 2012, **137**, 637.
- 61 N. Baffier and M. Huber, *J. Phys. Chem. Solids*, 1972, **33**, 737.
- 62 G. Singh, S. Gupta, R. Prasad, S. Auluck, R. Gupta and A. Sil, *J. Phys. Chem. Solids*, 2009, **70**, 1200.
- 63 H. T. Zhang and X. H. Chen, *Nanotechnology*, 2006, **17**, 1384.
- 64 X. Shi, S. L. Bernasek and A. Selloni, *J. Phys. Chem. C*, 2016, **120**, 14892.
- 65 H. Liu, X. Zhu, M. Li, Q. Tang, G. Sun and W. Yang, *Electrochim. Acta*, 2014, **144**, 31.
- 66 D. G. Wickham and W. J. Croft, *J. Phys. Chem. Solids*, 1958, **7**, 351.
- 67 H. Bordeneuve, PhD thesis, Université Toulouse III – Paul Sabatier, 2009.
- 68 G. Salek, PhD thesis, Université Toulouse III – Paul Sabatier, 2013.

MnCoO

Rémi Arras,^{*,†} Thi Ly Le,[‡] Sophie Guillemet-Fritsch,[‡] Pascal Dufour,[‡] and
Christophe Tenailleau[‡]

*CEMES, Université de Toulouse, CNRS, UPS, 29, rue Jeanne-Marvig, F-31055 Toulouse,
France, and CIRIMAT, Université de Toulouse, CNRS, INPT, UPS, 118 Route de
Narbonne, 31062 Toulouse Cedex 9, France*

E-mail: remi.arras@cemes.fr

*To whom correspondence should be addressed

[†]CEMES, Université de Toulouse, CNRS, UPS, 29, rue Jeanne-Marvig, F-31055 Toulouse, France

[‡]CIRIMAT, Université de Toulouse, CNRS, INPT, UPS, 118 Route de Narbonne, 31062 Toulouse Cedex
9, France

1 Co_3O_4 and Mn_3O_4

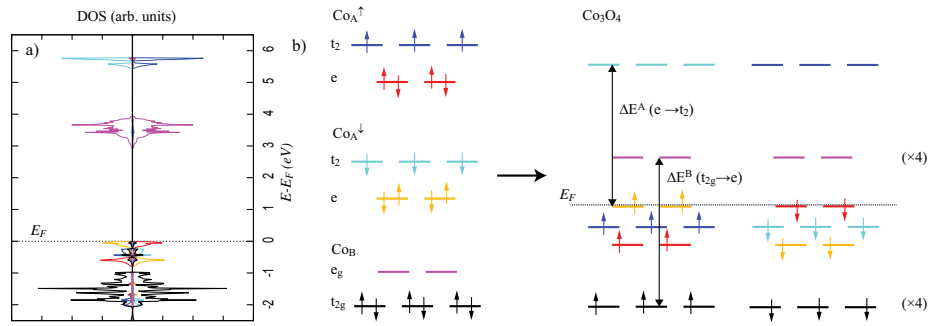


Figure 1S: a) Spin-resolved Co-d contribution to the DOS of Co_3O_4 , b) schematic representation of the electron distribution in the d orbitals.

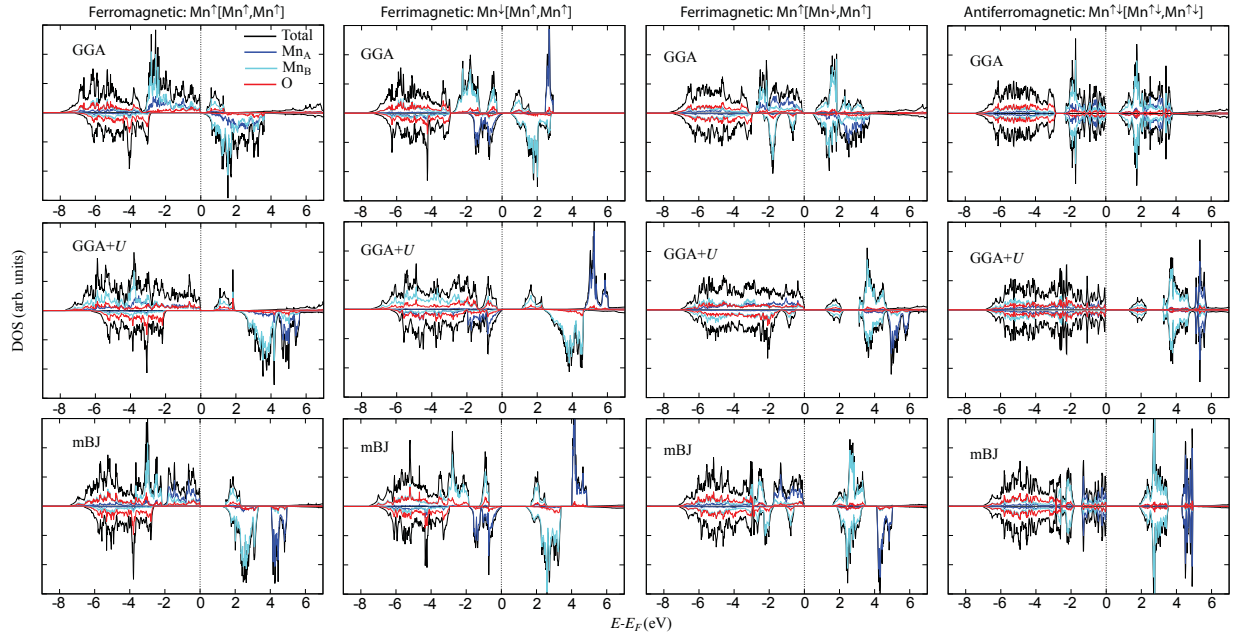


Figure 2S: Spin-resolved DOS for Mn_3O_4 calculated with the 3 approximations and for 3 different magnetic ordering.

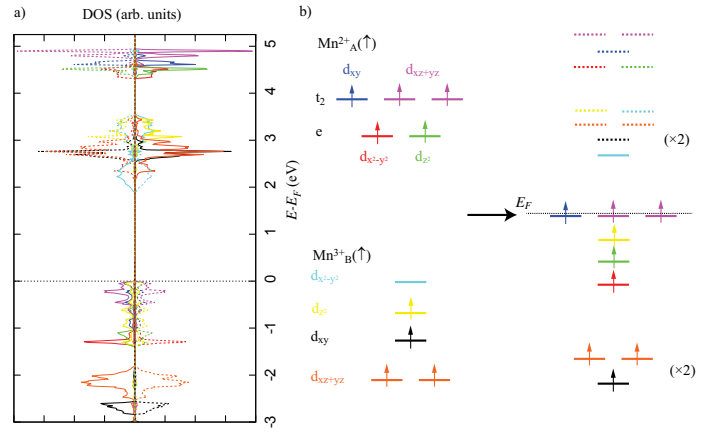


Figure 3S: a) Spin-resolved Mn-d contribution to the DOS of Mn₃O₄, b) schematic representation of the electron distribution in the d orbitals for one spin direction.

2 $\text{Mn}_x\text{Co}_{3-x}\text{O}_4$

2.1 Atomic structure

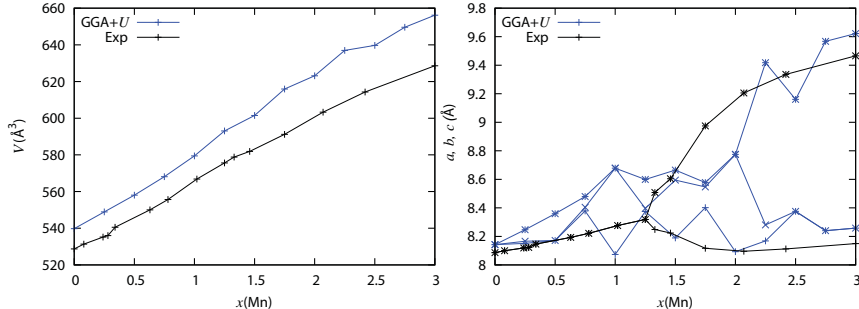


Figure 4S: Comparison of the volume and lattice parameters of $\text{Mn}_x\text{Co}_{3-x}\text{O}_4$ calculated with the GGA+ U method with the experimental measurements.

The GGA calculations may be inadequate to describe correctly the atomic structure of these compounds. It seemed however to be the most reliable solution owing to the problem of computational times and the difficulty to choose a good U_{eff} parameter. We indeed performed a calculations with the GGA+ U method, and found a more complex phase diagram than in GGA, with 3 different orthorhombic structures:

- with $a \sim b < c$ for $0 < x \leq 0.75$,
- with $a < b \sim c$ for $0.75 < x \leq 2.0$,
- with $a \sim b < c$ for $0 < x \leq 0.75$.

The small difference between a , b , and c can be due to the cation distribution, as we suggested it for the GGA calculations. In that case, the effect is much more noticeable. The lattice parameters are in general more sensitive to the cation distribution than with the GGA approximation. Moreover, instead of an underestimation of the volume, the GGA+ U method overestimates it.

However, it is difficult to distinguish, with this method, if the difference found with the measurements are only artefactual, due to a spurious cationic ordering coming from the

supercell description of the lattice, or if the lattice really adopt an orthorhombic shape (more probable here), with $a \neq b \neq c$. Also not discussed, but the angles can also slightly vary from the ideal 90° value (less than 1°). The GGA+ U calculations is not supported by our experimental measurements, but it can be consistent with the orthorhombic phase reported in some studies^{1,2} and calculations performed by other authors on manganites.³

2.2 Electronic structure

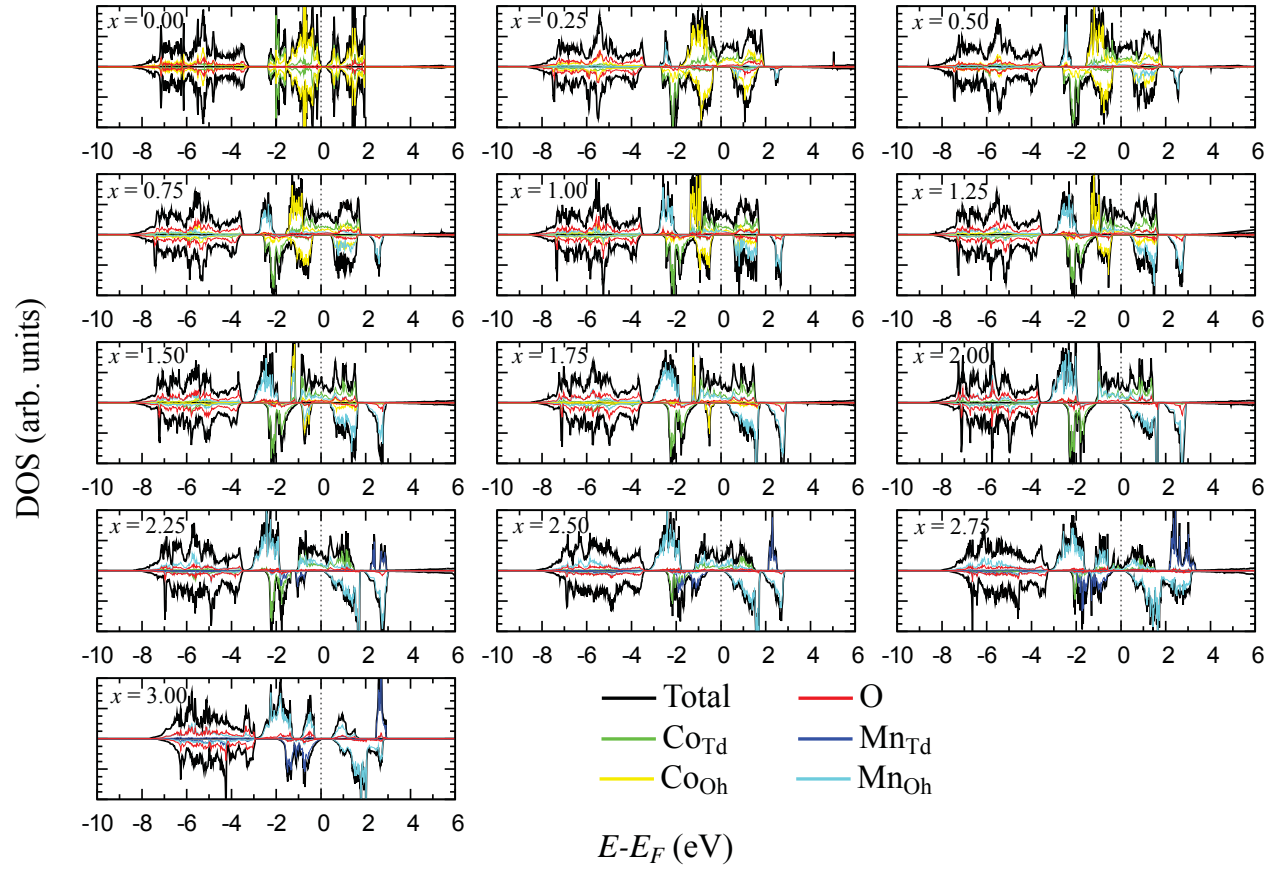


Figure 5S: Spin-resolved DOS for $\text{Mn}_x\text{Co}_{3-x}\text{O}_4$ ($0 \leq x \leq 3$) calculated with the GGA approximation.

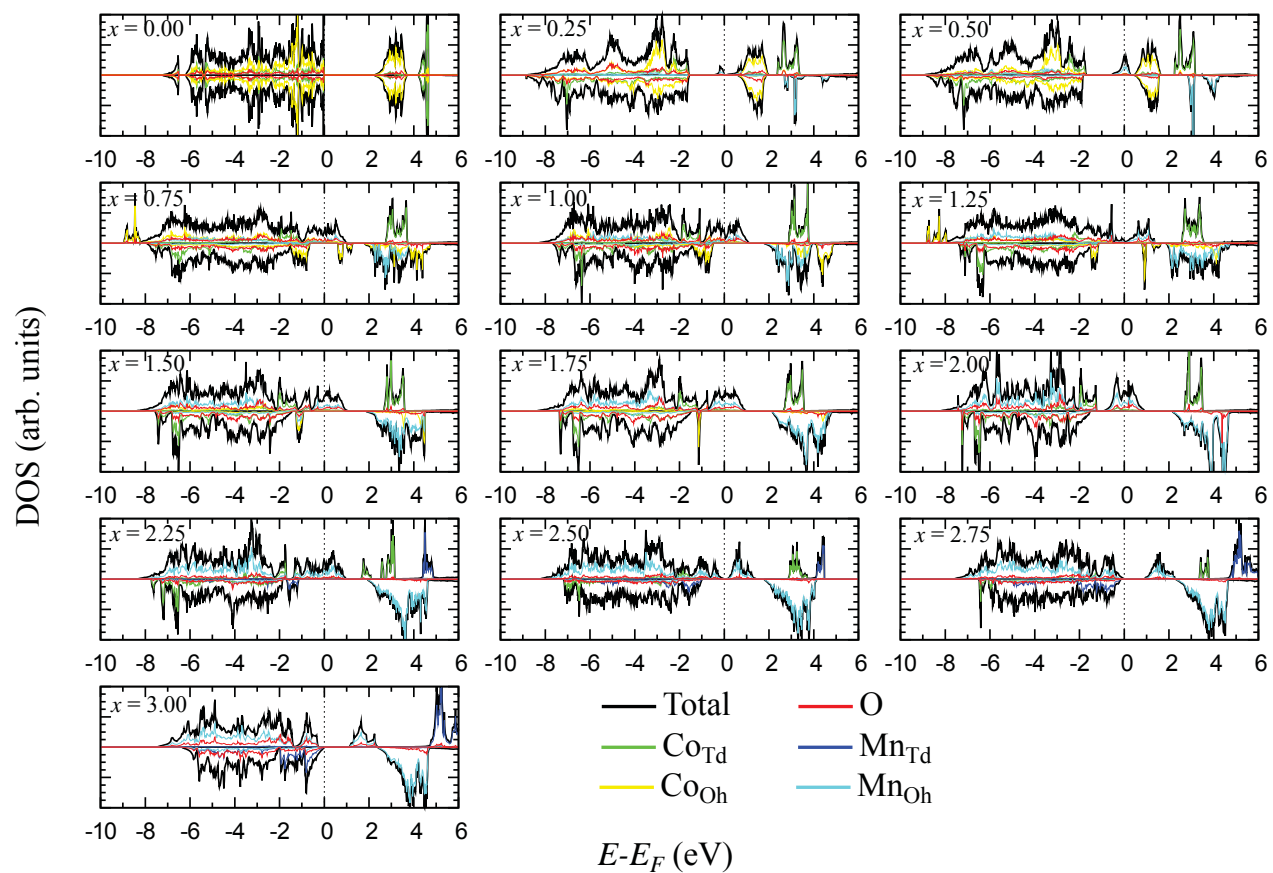


Figure 6S: Spin-resolved DOS for $\text{Mn}_x\text{Co}_{3-x}\text{O}_4$ ($0 \leq x \leq 3$) calculated with the GGA+ U approximation.

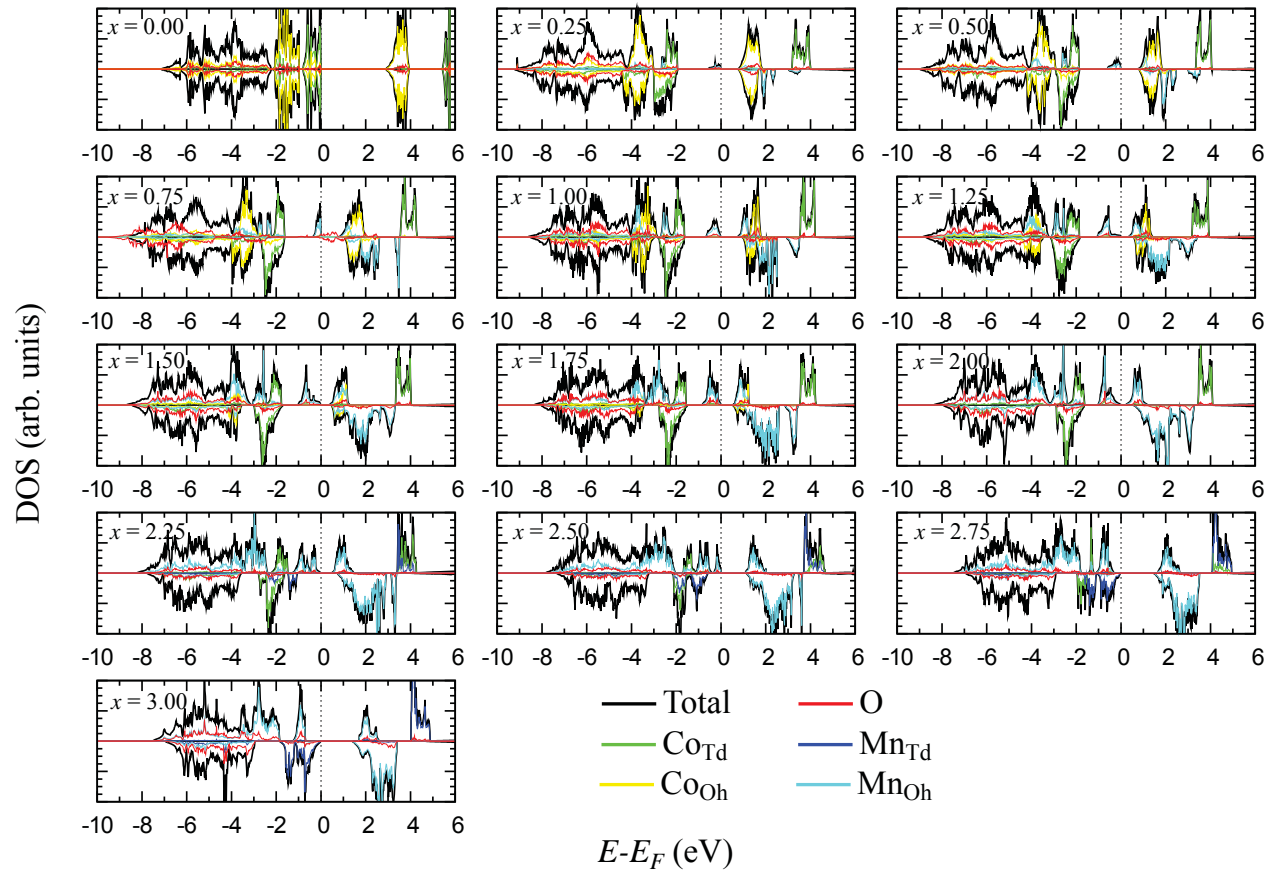


Figure 7S: Spin-resolved DOS for $\text{Mn}_x\text{Co}_{3-x}\text{O}_4$ ($0 \leq x \leq 3$) calculated with the mBJ approximation.

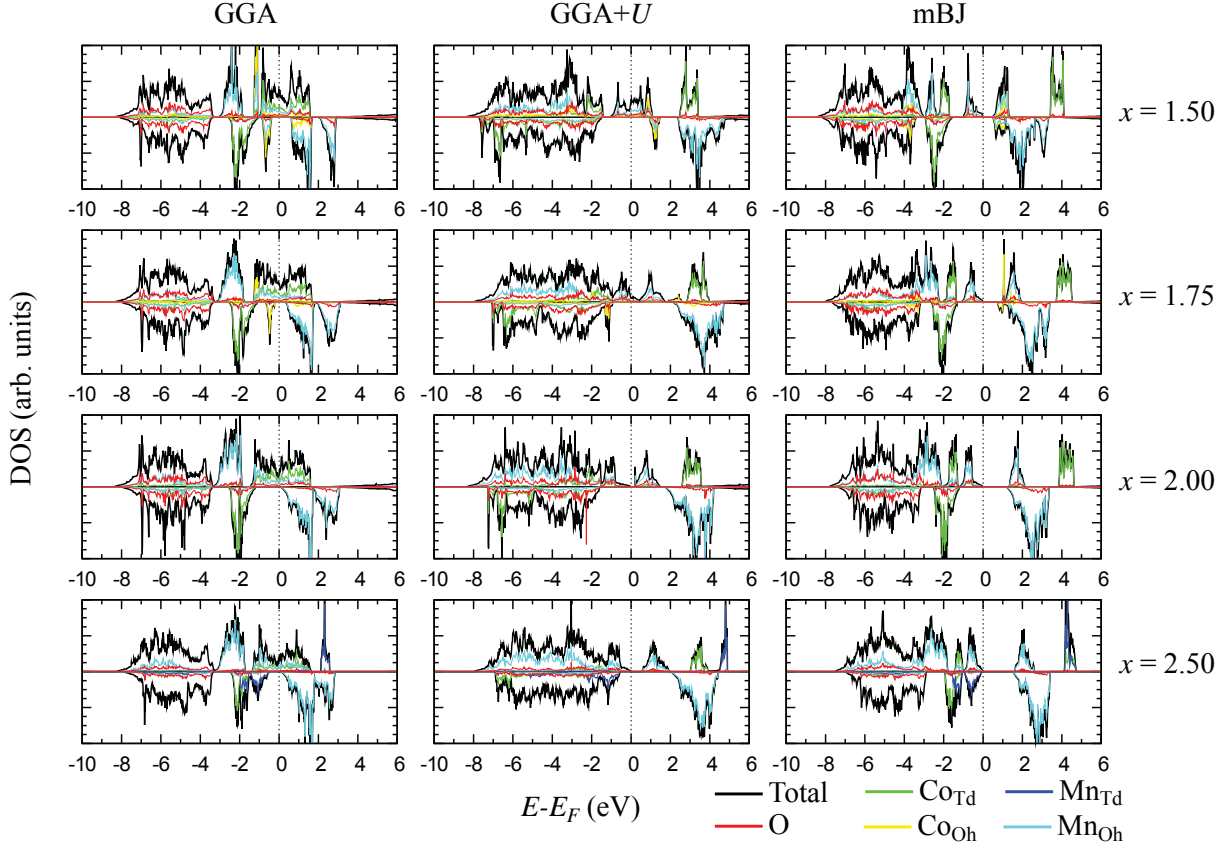


Figure 8S: Spin-resolved DOS for $\text{Mn}_x\text{Co}_{3-x}\text{O}_4$ ($1.5 \leq x \leq 2.5$) calculated with the experimental lattice parameters.

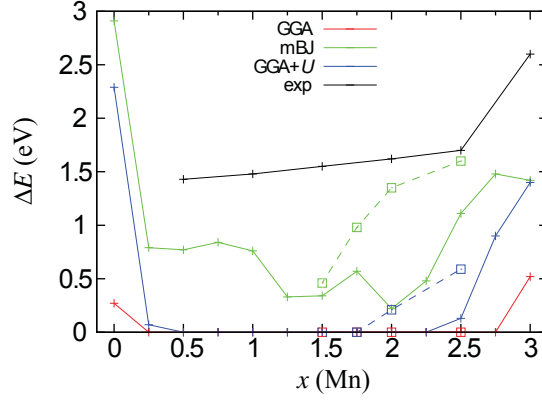


Figure 9S: Band gap energy as a function of x . Solid lines with + symbols corresponds to values obtained with the calculated lattice parameters, while dashed lines with \square symbols are the values calculated with the experimental lattice parameters.

Acknowledgement

This work was granted access to the HPC resources of CALMIP supercomputing center under the allocation p1313 (2014-2016).

References

- (1) Kim, M.; Chen, X. M.; Wang, X.; Nelson, C. S.; Budakian, R.; Abbamonte, P.; Cooper, S. L. *Phys. Rev. B* **2011**, *84*, 174424.
- (2) Kemei, M. C.; Harada, J. K.; Seshadri, R.; Suchomel, M. R. *Phys. Rev. B* **2014**, *90*, 064418.
- (3) Singh, G.; Gupta, S.; Prasad, R.; Auluck, S.; Gupta, R.; Sil, A. *Journal of Physics and Chemistry of Solids* **2009**, *70*, 1200.